Validation of braided-stream models:
Spatial state-space plots, self-affine scaling, and island shapes

Victor B. Sapozhnikov

St. Anthony Falls Laboratory, Department of Civil Engineering, University of Minnesota, Minneapolis

A. Brad Murray and Chris Paola

Department of Geology and Geophysics, University of Minnesota, Minneapolis

Efi Foufoula-Georgiou

St. Anthony Falls Laboratory, Department of Civil Engineering, University of Minnesota, Minneapolis

Abstract. We present a comprehensive approach for validating braided-stream models and apply it to a specific cellular braided-stream model. The approach involves quantitative comparison of modeled and natural braided streams in terms of two main aspects: the sequential organization of their plan patterns studied using their state-space characteristics and the hierarchical organization of their patterns studied in the framework of self-affine scaling. These two aspects of braided streams are complementary to each other and taken together provide a sensitive test of the validity of a model of braided streams. The simple model we examine produces patterns that are similar to those of natural braided rivers in terms of both sequential organization and self-affine scaling. This finding supports the conclusion that the nonlinear interactions between water and sediment in the model are the primary mechanisms responsible for shaping braided rivers in nature.

1. Introduction

A new computational model for fully developed braided streams has been proposed recently by *Murray and Paola* [1994]. Water and sediment are routed from cell to cell in a computational grid using simple abstractions of the governing conservation equations for mass and momentum. The model appears to reproduce the main dynamic features of stream braiding: formation of multiple interwoven channels separated by islands within which the flow shifts continuously from path to path, reshaping the islands as it does so. The model also reproduces broadband fluctuations in sediment discharge that have been observed in laboratory and field braided rivers.

Given the simplicity of the model, its ability to reproduce many features of real braided rivers even at a qualitative level is encouraging. But how does one test such a model quantitatively? In many systems whose spatial patterns possess one or more well-defined characteristic length scales, the first test is to see how well the model results match these scales quantitatively. However, recent work by *Sapozhnikov and Foufoula-Georgiou* [1996, 1997] has shown that braided rivers exhibit self-affine scaling in their morphology and that their temporal dynamics is consistent with self-organized critical behavior. These results suggest that braided rivers do not possess characteristic length scales, either when viewed as static spatial patterns or in terms of their temporal evolution. What is the best way to test models of such a system?

In this paper, we present a comprehensive approach to testing braided-stream models on the basis of two main aspects:

the sequential organization and the hierarchical organization of their plan patterns. These two aspects of braided streams are complementary to each other, as the first depicts the river pattern in the dynamical-system theory framework and the second one describes scale-invariant characteristics of the braided-stream system.

Before discussing the technical details of the model and the various tests, a brief overview of the philosophy of the various approaches for model validation of a complex, scale-invariant system may be helpful. The basic question in model validation is, what are the features of the system of interest that are truly fundamental and give it its distinctive character? For instance, there is an extensive body of literature describing stability theories of stream meandering [e.g., see *Parker*, 1976; *Fredsoe*, 1978]. Two basic criteria are used to evaluate these theories: correct prediction of the physical conditions needed to produce meandering (primarily in terms of channel width-depth ratio) and correct prediction of the ratio of meander wavelength to channel width. These criteria are appropriate for such systems because meandering has a clear, dominant wavelength; indeed, the requirement of a preferred wavelength is embedded in the whole notion of stability analysis [*Parker*, 1976; *Fredsoe*, 1978], in which the single most unstable wavelength is presumed to dominate the fully developed system. Although the initial development of a braided pattern from a straight channel does appear to involve a single dominant bar wavelength, as described in stability theories, the picture for fully developed braiding is quite different. The original regular pattern of bars breaks up into a complex network of bars and channels on many length scales. Though it appears to remain statistically stationary (given constant flow conditions), the network continually reconfigures itself. The spatial pattern at any instant is "self-affine," that is, shows an anisotropic fractal
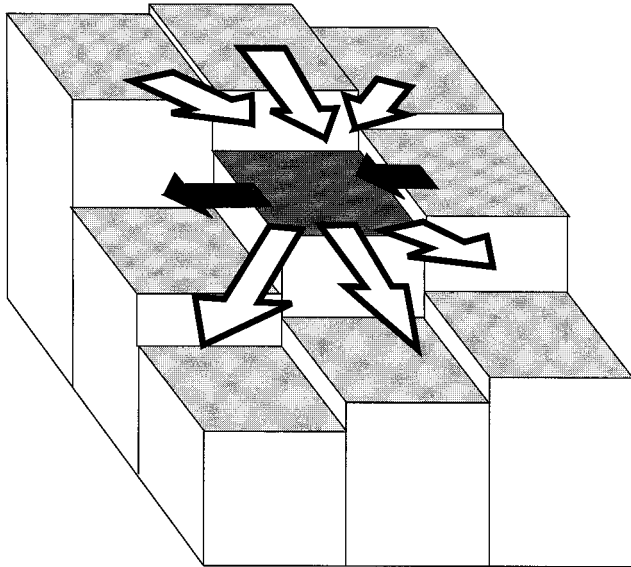
Figure 1. A schematic illustration of the rules in the cellular braided-stream model. Open arrows represent water routing and downstream sediment transport, and solid arrows represent the lateral-transport rule.

geometry in which patterns at different magnification scales are statistically similar within a consistent stretching of one spatial coordinate relative to the other. Like self-similar (isotropic) fractals, self-affine systems have a hierarchical geometric organization but no characteristic length scale (up to the scale of the whole system). The transition from an initial instability with a well-defined dominant wavelength to the final scale-free configuration is not well understood, but it may be analogous to the transition in fluids from an initial single-wavelength instability to the broadband distribution of eddies that characterizes fully developed turbulence [e.g., see *Tennekes and Lumley*, 1990].

The model developed by *Murray and Paola* [1994] is aimed not at predicting the conditions of formation of initial instabilities that might lead to braiding, but at the properties of the fully developed braided state. Hence model comparisons with initial bar wavelengths would not be very useful. Instead, model comparisons employing measures of spatial patterns and temporal dynamics would be more appropriate. Such measures, which include self-affinity in morphology, scaling behavior of island shapes, and dynamic scaling in spatiotemporal structure, capture information about the hierarchical space-time organization of the pattern: the relation of the whole to the parts of which it is made.

Another line of analysis is suggested by the fact that the flow of water down a river implies a preferred direction of causality. Under these conditions a spatial series is directly analogous to a time series, opening the possibility of applying the many techniques that have been developed for analysis of chaotic time series [*Weigend and Gershenfeld*, 1994; *Takens*, 1981; *Sauer et al.*, 1991; *Sugihara*, 1994]. Here the analysis aims to capture information about the sequential organization of the plan pattern: how the pattern at one point in space depends on the pattern upstream. We focus on spatial series of total flow width because they are readily measured from aerial photographs. Of course, total flow width is an aggregate measure of the morphology of a braided river, and as such it does not

explicitly carry information about the relative position, shape, and distribution of widths of individual channels. This information, however, is explicitly incorporated in the self-affinity tests which look statistically at the detailed planform geometry of the braided patterns.

2. Summary of Cellular Model

In a cellular model, called a "coupled map lattice" by *Kaneko* [1993], the cells of a lattice interact according to simple rules meant to represent the basic physics of a system. Cellular automata models have found a wide application in the physical sciences [e.g., see *Vichniac*, 1984; *Toffoli*, 1984; *Salem and Wolfram*, 1986; *Frish et al.*, 1986], and such a model was proposed by *Murray and Paola* [1994, 1997]. Here we give only a brief overview of the model.

Elevations are defined for each cell in the lattice, initially forming an overall slope with random elevation perturbations which are the only random input into the model. At each iteration, water is introduced into cells at the uphill end of the lattice. From each cell the water is distributed to the three downstream immediate neighbor cells, with more water going where the bed slopes are steeper (Figure 1). A rule relates the amount of sediment transported from a cell to one of the three downstream neighbors, Q_{si}, to the local slopes and discharges. *Murray and Paola* [1994] have employed several sediment-transport rules, but here we will not consider rules that produce visually unrealistic patterns or contain terms that do not enhance the pattern's apparent realism. We will refer only to the rules called Q_s rules 3 and 4, respectively.

$$Q_{si} = K(Q_i S_i + Q_i C)^m \qquad (1)$$

$$Q_{si} = K\left(Q_i S_i + \varepsilon \sum_j Q_j S_j \right)^m \qquad (2)$$

where K is a constant and Q_i and S_i are the discharges and slopes from the cell in question to downstream neighbor i. In Q_s rule 3, C is a constant. In Q_s rule 4, ε is a constant, and Q_j and S_j refer to the discharges and slopes from the three upstream neighbors into the cell in question. $Q_i S_i$ is the stream power index. The terms added to the stream power index in Q_s rules 3 and 4 allow sediment to be transported on locally flat or slightly uphill slopes, as occurs locally in real rivers, as long as water continues to flow downstream into the cell in question. On the basis of *Ashmore*'s [1985] compilation of data from laboratory and natural gravel bed rivers with a range of stream powers, we estimate that the whole river sediment transport varies as the reach-averaged stream power raised to an exponent of approximately 2.5. Although this does not apply strictly to the local treatment of sediment transport in the model, with the terms added to the stream power, we use 2.5 as a reasonable value for the exponent m. Model results do not depend sensitively on the value of m [*Murray and Paola*, 1997]. Another rule transports a small amount of sediment down transverse slopes (Figure 1) [*Murray and Paola*, 1994], representing the gravity-induced component of bedload sediment transport that occurs in real rivers when the bed slope is not parallel to the flow direction [*Blondeaux and Seminara*, 1985; *Parker*, 1978, 1984]. When the water reaches the downhill end of the lattice, the iteration ends, and the elevation of each cell is adjusted according to the difference between the amount of sediment entering and leaving that cell.

The output of the model is the distribution of water dis-

charge and bed topography over the lattice as a function of time. Both quantities can be measured in the laboratory, though only the general pattern of flow distribution (i.e., presence/absence) can be readily obtained from field aerial photographs. Sediment flux is also computed in the model, but since spatial distribution of sediment flux is difficult to measure in the field, we have not used it as a comparison variable.

3. State Space Approach

As discussed in section 1, one approach to evaluating the realism of a given model is to see how well it describes the sequential structure of real systems. In real braided rivers the geometry of the flow at one point affects the geometry that develops downstream. For example, where the flow is confined in a single narrow, deep channel, the sediment flux into downstream areas will likely be relatively large. This large flux enhances the likelihood that deposition and bed aggradation will occur where the channel next widens. Deposition often causes the flow to become wider and shallower. The downstream decrease in local flow strength heading into the shallow section encourages further deposition. Thus wide shallow flows and midchannel bars often occur directly downstream of narrow, deep sections in braided streams. If the processes in the model are similar to those in real braided streams, the downstream influences should be similar, leading to similar sequences of downstream changes in geometry.

We parameterize the geometry of braided streams by measuring total widths (the sum of the widths of all the channels in a cross section) for a long series of cross sections. (Other geometric variables could be used [*Murray and Paola*, 1996], but widths for many cross sections can be measured from aerial photographs. In addition, because it is the sequences of widths that are of interest, changes in stage should not affect the results strongly.) Constructing a spatial "state-space plot" by plotting each total width versus the previous width (or versus more than one previous width in higher-dimensional plots) encapsulates the information about the downstream changes in widths in that section of river (Figure 2). *Murray and Paola* [1996] described one method for quantitatively comparing state-space plots. Using this to compare plots representing model-generated and real patterns provides a measure of how realistic the model is. Here we improve on this approach in two ways. First, *Murray and Paola* [1996] used width data from two braided streams. Here we present data from an additional river which differs in characteristics such as slope and sediment type, providing a more reliable basis for comparison. Second, we apply a new method for quantitatively comparing state-space plots [*Moeckel and Murray*, 1997], which is more robust than the one applied previously.

3.1. Comparison Method

The technique of plotting each value in a time series versus some number of previous values is called "delay coordinate embedding" in dynamical-systems research [*Takens*, 1981; *Sauer et al.*, 1991]. As the system moves from one point in the plot, representing the current value and the recent past, to successive points, the system traces out a path through the state space. For a system that is deterministic and involves a small number of important variables, and yet displays complex and unpredictable behavior (a "chaotic" system), delay coordinate embedding is one way to depict the system's "attractor." An attractor is the manifold in state space (also called "phase
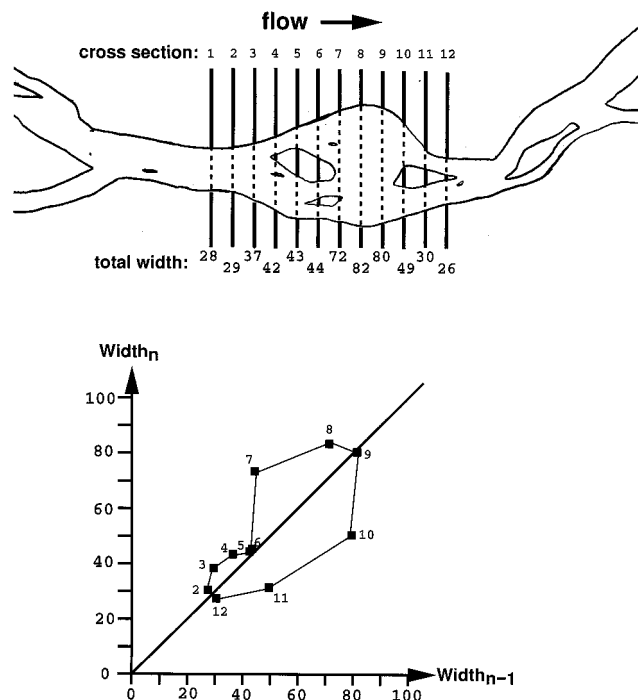

Figure 2. An illustration of how a two-dimensional state-space plot is constructed from a series of total widths. Total widths are the sum of the widths of all the channels in a cross section. A width greater than the previous width plots above the diagonal and vice versa. The magnitude of the difference between the two widths determines how far from the diagonal the point falls.

space") that the system moves on as its long-term behavior is plotted. Superficially different time series from the same system will trace out very similar patterns, which depict the sequences of changes the system exhibits. To produce an accurate representation of the attractor, the plot must be of sufficiently high dimension; each point must represent enough previous values to uniquely determine the next value and therefore the next point. This means that in such a plot of a deterministic system, lines connecting successive points will not cross.

Plotting a spatial series of braided-stream total widths using delay-coordinate embedding in two or three dimensions produces patterns with lines that often cross (Figure 3). In other words, the downstream influences are not deterministic in these few dimensions; a sequence of three total widths is not enough information to uniquely determine the next width. This system may appear more deterministic in higher dimensions, or it may include some stochastic behavior. However, the method we use for quantitatively comparing state-space plots does not require that the system be plotted in the proper dimensions or that it be deterministic; the plots are not assumed to depict attractors. This method treats state-space plots as probability distributions, comparing the frequency with which typical sequences occur. In this context, the state-space–plot comparison method does not require that a given sequence of total widths is always followed by the same width. This method provides a useful way to compare spatial series of widths as long as there is enough downstream influence to produce typical series of widths rather than completely random series.

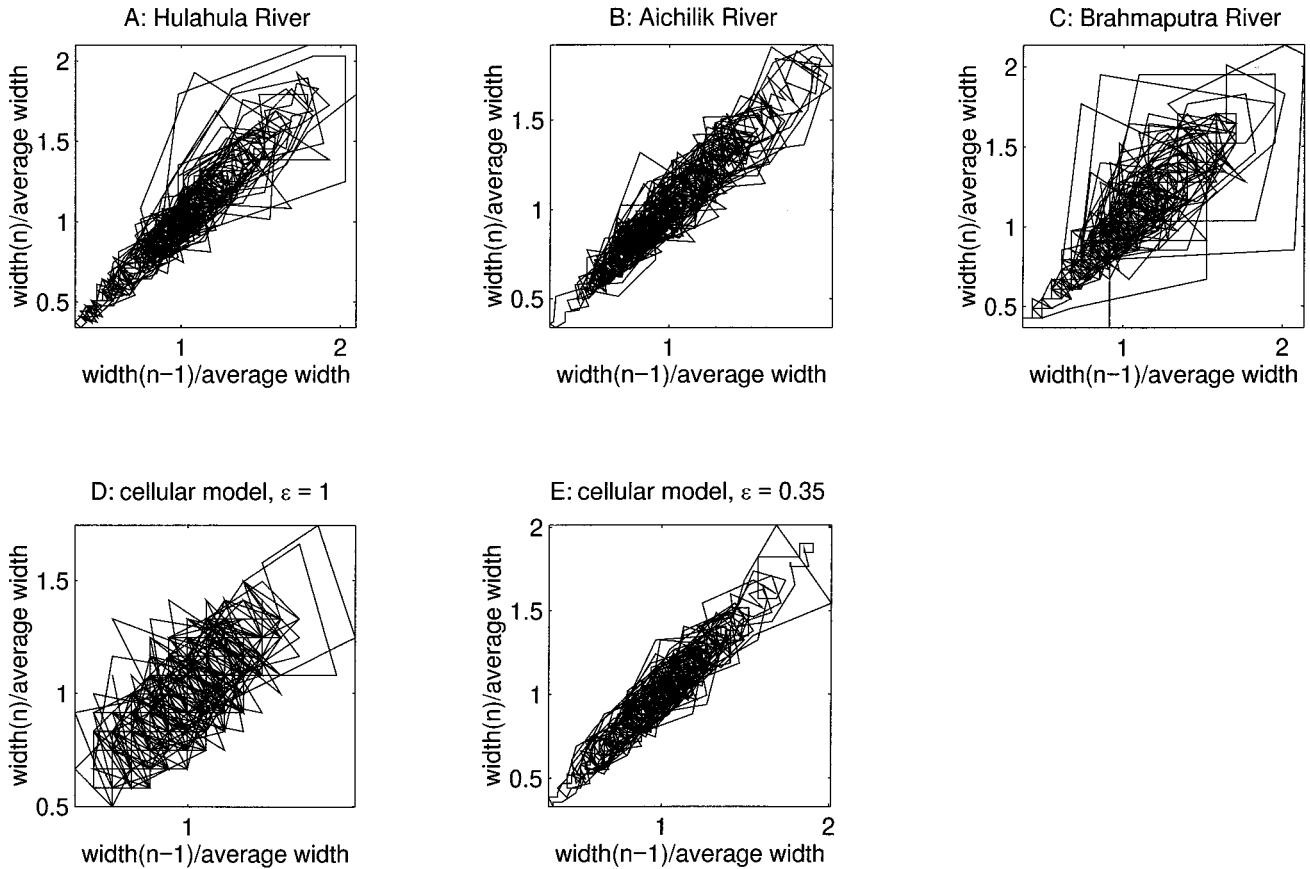In the first step of this method, state-space plots are trans-

Figure 3. State-space plots of total-width series from (Figures 3a–3c) real rivers and (Figures 3d and 3e) the model runs. Each data set is normalized to the average total width for the reach measured.

formed into discrete probability distributions by dividing the state space into cells and assigning a probability to each cell that is equal to the number of points in that cell normalized by the total number of points in the plot. Then an algorithm finds the minimum average distance that the elements of one discretized distribution must be moved to duplicate the other distribution (Figure 4). The distance is given in the units in which the series are expressed. This metric was proposed originally by Kantorovich as an optimal solution of transportation problems and was later applied in the probability literature [*Dudley*, 1989]. *Hutchinson* [1981] used a related function in connection with iterated function systems. *Moeckel and Murray* [1997] adapted the theoretical metric into a practical comparison between discretized probability distributions. The probabilistic and geometric properties of this "transportation distance" give it advantages over other commonly used metrics for assessing how similar the arrangements of probability in two distributions are, which represents in this case how similar the typical sequences in two series are. For example, the transport distance is relatively insensitive to outliers, especially when compared to the Hausdorff distance [*Moeckel and Murray*, 1997]. In addition, if corresponding areas of high probability do not fall in quite the same state-space location in two distributions, the transport distance's geometric properties make it sensitive to how far apart the two areas are. In contrast, the Kolmogorov metric does not directly measure such differences [*Dudley*, 1976]. The transportation distance is much less sensitive to the cell sizes used in the discretization of the state space, and to perturbations in the series, than is the method

used by *Murray and Paola* [1996] in the preliminary test of the braided-stream model [*Moeckel and Murray*, 1997].

3.2. Similar Plots From Different Kinds of Braided Streams

Measuring a long series of widths under uniform conditions requires a long reach of a river without tributaries, topographic
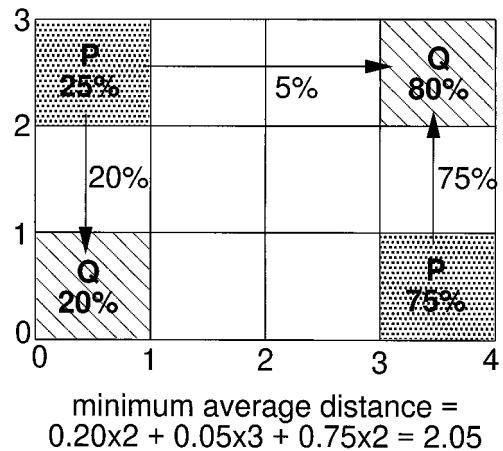

minimum average distance = 0.20x2 + 0.05x3 + 0.75x2 = 2.05

Figure 4. A simple illustration of the transportation distance between the discretized probability distributions P and Q. Numbers next to arrows show how much probability is transported in each step of transforming P into Q. If the distributions overlapped in some cells, the total of these numbers would be less than 100%.

obstacles, changes in slope, or changes in grain size. We have found such reaches on two gravel-bed braided rivers, the Aichilik and Hulahula Rivers on the North Slope of the Brooks Range in Alaska, and on one sand-bed river, the Brahmaputra River in Bangladesh. On the gravel rivers, measurements of surface grain size, using the method of *Wolman* [1954], show no significant downstream grain-size changes on the gravel-bed rivers (for Aichilik data, see *Murray and Paola* [1996]). We have not performed any field studies of the Brahmaputra. We also use data from a laboratory-scale braided stream that exhibits Froude number similarity to a gravel-bed braided river. We traced the discharge pattern of the Brahmaputra from a satellite image that had a poorer resolution relative to the river's size than the aerial photographs used for the other two rivers or the overhead photographs used for the laboratory stream. As a result, the smallest channels in the Brahmaputra were not traced.

These braided streams differ greatly in relative grain size, slope, and scale of flow (Table 1). One might expect that such different streams would have fundamentally different patterns (patterns that had very different typical downstream sequences of total widths, for instance). However, Figures 3a–3c show that all the plots of each total width versus the previous width are quite similar. Widths are normalized to units of the average total width $\overline{w_T}$ for each river, and cross sections have approximately the same relative spacing for each river (0.08 $\overline{w_T}$). Some of the details of these plots differ, especially in the presence or absence of a few wide loops, which show occasional abrupt downstream width changes. However, the areas where the data are dense in these plots are similar, indicating similar typical sequences of widths. A plot with these characteristics is not inevitable for any braided pattern; Figure 3d shows the results of a run of the braided-stream model that produces a braided pattern that does not result in a plot like those for the real streams. For instance, this plot extends farther from the diagonal in the lower left, indicating more abrupt downstream width changes when the width is relatively small. In addition, the model plot does not extend as far along the diagonal, reflecting a smaller variance in the widths.

Because the geometry at one cross section influences the geometry at successive sections via the mechanisms of flow and sediment transport, the similar sequences of widths shown by the plots in Figures 3a–3c suggest that fundamentally similar mechanisms operate in all these braided streams. Perhaps the

Figure 5. Transportation distances between the probability distribution representing the Hulahula River and those representing model runs with different values of ε in Q_s rule 4. Each point is an average over two to four snapshots of the model. The braid plain is 46 × 1000 cells in each run. (In section 3 we discuss the fact that some aspects of the model patterns using this sediment-discharge rule appear not to reach steady state until ~100,000 iterations. In this experiment we used snapshots from 20,000–65,000 iterations. However, in these runs, discharge is introduced in each cell in the first row, rather than in one fourth of the cells as in all the other model runs we discuss. The relatively larger discharge means that more material is moved each iteration, so that the patterns develop faster [see *Murray and Paola*, 1994]. In addition, larger values of ε mean that more material is transported in each iteration. We used snapshots from as few as 20,000 iterations only in the largest-ε runs.)

large-scale interactions between flow and sediment are insensitive to the differences in relative grain size and flow characteristics among these streams. The state-space plots of downstream changes in width summarize what appears to be a robust, important aspect of real braided-stream patterns that can be used as a basis for model comparison.

3.3. Quantitative Model Evaluations

Moeckel and Murray [1997] demonstrated that the transportation distance method of comparing state-space plots can be used to find the optimal value of an unconstrained model parameter. The term that allows sediment transport on flat and slightly uphill surfaces in Q_s rule 3 is physically motivated; flow momentum and therefore sediment transport should increase with increasing slopes and discharges into an area. However, the magnitude of this term, determined by ε, is only loosely constrained [*Murray and Paola*, 1994]. Figure 5 shows how the model realism varies with ε. Realism is measured here by the transportation distances between the state-space plot representing the Hulahula River and the plots representing the model. We show the results using the Hulahula data because it is the longest of our data sets (the longest reach, in units of the average total width, with uniform conditions), but experiments using other data sets show very similar results. Widths in the model are the number of cells in a cross section with discharge greater than a cutoff, which is 0.35% of the total discharge in these runs. Each data point in Figure 5 represents an average over two to four snapshots between 30,000 and 50,000 itera-

Table 1. Hydrologic and Geomorphologic Characteristics of Brahmaputra, Aichilik, Hulahula, and Tanana Rivers

	Brahmaputra	Aichilik	Hulahula	Tanana
Reach width, km	15	0.5	0.7	1.8
Reach length, km	200	6.4	20	28.6
Mean channel depth, m	5	1	1	—
Slope	0.000077	0.001	0.0007	0.001
Braiding index*	3.8	6.8	5.2	4.6
Predominant type of the bedload	sand	gravel	gravel	gravel + sand
Fractal exponent ν_x	0.74	0.72	0.74	0.70–0.77†
Fractal exponent ν_y	0.51	0.51	0.52	0.47–0.50

*The braiding index (BI) for each river was computed as the average number of channels in cross sections of the photo image of the river.

†The fractal exponents for the Tanana River were estimated at three different times (different stages of the river).
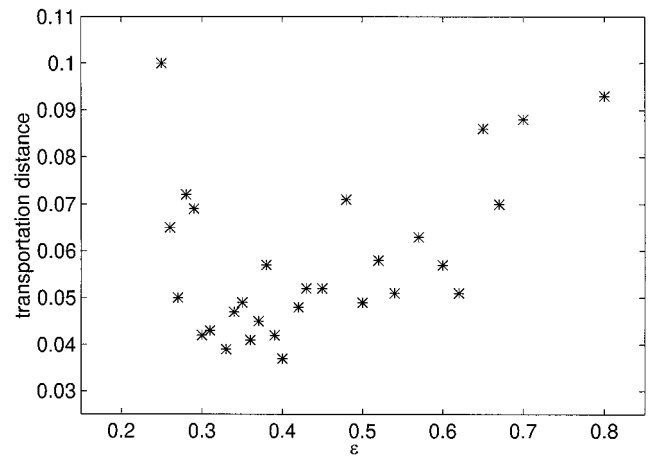
$$Q_S = (Q)^m, \; m = 2$$

A: flow divergence ⟶ deposition
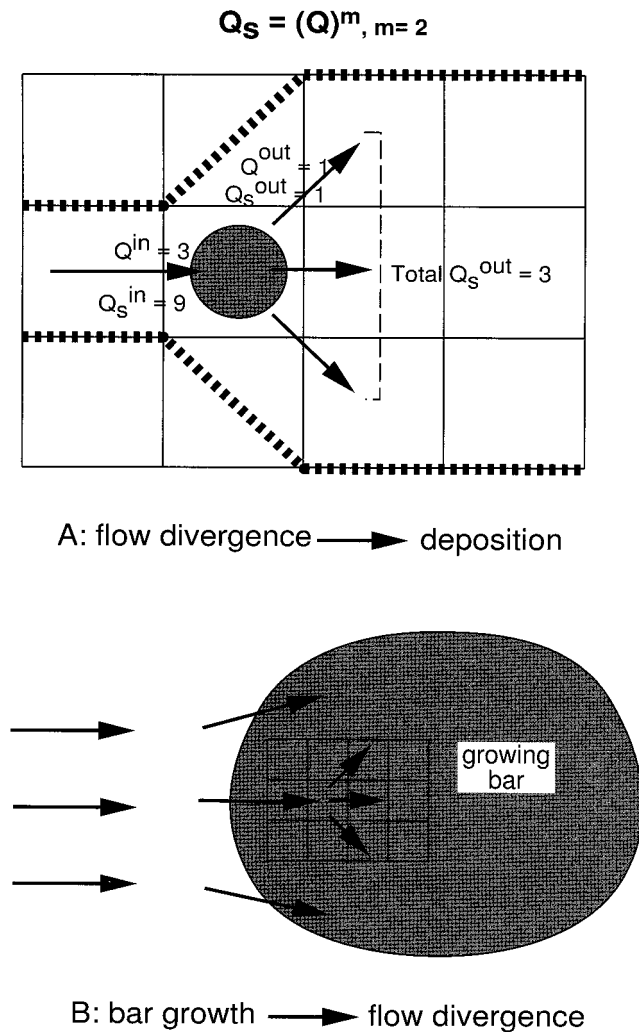

B: bar growth ⟶ flow divergence

Figure 6. Schematic illustration of the effects of the nonlinear dependence of sediment transport on discharge in the model. For simplicity, in Figure 6a the slopes are assumed to be constant, so that the discharge spreads evenly into the downstream cells at the divergence. In this case, sediment transport is proportional to discharge raised to the power of m for either Q_s rule 3 or 4. We use $m = 2$ and a constant of proportionality of 1 for further simplicity. Figure 6b illustrates how a growing bar causes flow divergence and therefore a situation similar to that depicted in Figure 6a.

tions, with lattice dimensions of 1000×46 cells. The transportation distance reaches a minimum at a value of ε 0.3–0.4.

Figures 3a–3c and 3e show that the state-space plot of a model run using this value of ε shares the main characteristics of the plots of the real rivers. In the model the mechanism that is most essential to produce braiding is the nonlinear dependence of sediment transport on flow strength, specifically discharge, with the exponent $m > 1$ in the Q_s rule [*Murray and Paola*, 1994]. With this relationship, flow divergences tend to produce convergence in the sediment flux and therefore local deposition. Figure 6 illustrates this for a simple case and shows how the feedback of deposition enhancing flow divergence can lead to bar formation. The nonlinear relationship also causes the opposite instability; flow convergence tends to produce erosion and bed lowering, which enhances flow convergence at that location. The slope dependence of the stream power tends

to oppose these instabilities. For example, it decreases the amount of sediment transported across the reduced or negative slopes out of low areas and onto barheads. The term that allows sediment transport over flat or slightly uphill slopes partially offsets this effect in the model, making it easier for sediment to move from a deep (and therefore usually narrow) section into an area of flow divergence and bar formation. We suggest that these large-scale mechanisms are also the most important processes in real braided streams, leading to the similarity in the downstream changes in width between real rivers and the model.

Table 2 shows, for each of several model images, the average transportation distance between that image and each of the three natural rivers. (The laboratory-stream data set has fewer points than any of the real-river data sets, so we leave it out of this analysis.) Seven of these model snapshots are from two different runs that used Q_s rule 4 with the optimal ε value (0.35). (These runs differed in the side boundary conditions: Q_s rule 4 run B had erodible banks between the braid plain and high side walls. These banks were not present in Q_s rule 4 run A. The braid plains in both runs spanned 1500×100 cells.) The transportation distances in Table 2 are slightly lower than the minimum shown in Figure 5 because for these images we traced the model output in the same way as we did for the natural patterns. Rather than automatically measuring the total width as the number of cells in a cross section with discharge above a cutoff, we applied the same standards to model patterns that we applied when tracing the real-river patterns. For instance, noncontinuous channels were not included in the patterns. The mean value of the transportation distance between real-river plots and all the images produced with Q_s rule 4 is 0.038, with a standard deviation of 0.014, in units of average total width.

Quantitatively assessing how realistic the width sequences in the model are requires a benchmark to judge this mean against. Table 3 lists the transportation distances between plots representing the three natural rivers. These distances measure the variability in typical sequences not only between different realizations of natural rivers but also between different types of natural rivers. The model is too simple to be a simulation of one of the types of rivers specifically; there is no explicit grain size or slope, for example [*Murray and Paola*, 1997]. The best that could be hoped for is that the plots representing model patterns match those representing real rivers as closely on average as the real-river plots match each other. The average distance between real-river plots is 0.026, with a standard deviation of 0.003 (Table 3). The difference between this value and the average transportation distances between model plots and real rivers (Table 2) suggests that the model does not always match the real rivers as closely as real rivers match each other. Although the sizes of the data sets are smaller than would be desired for a rigorous statistical treatment, we applied a two-sample Welch's t test, which measures the likelihood that two groups of numbers could really be derived from the same population, given the means, standard deviations, and number of samples in each group [*Miller*, 1986]. This test indicates that there is less than a 0.1% probability that the difference between the two means is not meaningful. This number should not be considered exact, because the assumption behind the test, that the underlying populations from which the samples are drawn are normally distributed, has not been proven to be valid. However, slight deviations from normality are unlikely to alter the basic conclusion that the model

Table 2. Transportation Distances Between Model and Real-River Plots and Scaling Statistics of Model Images

Model Image	Transportation Distances				Scaling Characteristics	
	Hulahula	Aichilik	Brahmaputra	Average	ν_x/ν_y	D
Q_s rule 3 87,000 iterations	0.044	0.029	0.039	0.034	1.55	1.50
Q_s rule 3 90,000 iterations	0.033	0.025	0.035	0.031	1.46	1.47
Q_s rule 3 138,000 iterations	0.034	0.027	0.040	0.035	1.95	1.62
Q_s rule 3 145,000 iterations	0.045	0.034	0.038	0.038	1.65	1.69
Q_s rule 4, run A 61,000 iterations	0.021	0.018	0.050	0.029	$\cdots$	1.48
Q_s rule 4, run A 105,000 iterations	0.070	0.052	0.054	0.057	1.63	1.57
Q_s rule 4, run A 169,000 iterations	0.043	0.034	0.048	0.038	1.44	1.53
Q_s rule 4, run B 91,000 iterations	0.034	0.016	0.034	0.028	$\cdots$	1.57
Q_s rule 4, run B 134,000 iterations	0.034	0.029	0.042	0.033	1.39	1.60
Q_s rule 4, run B 172,000 iterations	0.030	0.040	0.059	0.044	$\cdots$	1.78
Q_s rule 4, run B 181,000 iterations	0.023	0.022	0.043	0.030	1.88	1.74

Run B had erodable banks between the braid plain and high side walls. These banks were not present in run A.

is probably not completely realistic. This is not surprising given the simplicity of the model.

Murray and Paola's [1996] preliminary analysis suggested that runs using Q_s rule 3 produced patterns with width sequences that were less realistic than those produced with Q_s rule 4. However, using the transportation-distance method of comparing state-space plots and the larger number of real-river data sets, Q_s rule 3 patterns match the real rivers at least as well as the Q_s rule 4 patterns do, on average; the average distance between plots representing these patterns and those representing real rivers is 0.035, with a standard deviation of 0.006 (Table 2). Applied to the mean for Q_s rule 3 patterns, the two-sample t test gives a <0.1% chance that this mean could be found for a sample of this size of the within-real-river population.

State-space plots of total widths characterize an important aspect of braided-stream patterns. However, this approach is not sensitive to the arrangement or number of channels. Section 4 addresses the realism of these aspects of the model patterns by analyzing self-affine scaling properties and channel shapes.

4. Self-Affine Scaling Approach

In a recent study, *Sapozhnikov and Foufoula-Georgiou* [1996] examined the spatial patterns of three natural braided rivers (aerial images of the Aichilik and Hulahula Rivers in Alaska and the satellite images of Brahmaputra River in Bangladesh)

Table 3. Transportation Distances Between Real-River State-Space Plots

River	Aichilik	Brahmaputra
Hulahula	0.022	0.030
Aichilik	$\cdots$	0.027

and found that they exhibit anisotropic scaling (self-affinity). Similar results were obtained more recently for the Tanana River in Alaska using synthetic aperture radar (SAR) data [*Nykanen et al.*, 1998]. Self-affinity in a braided river implies that if a small part of the braided river is stretched differently in the direction of the river slope and in the perpendicular direction, then the stretched part looks statistically similar to a larger part of the braided river. Despite the large differences in scales (0.5–15 km), slopes (7×10^{-3} to 8×10^{-5}), and bed material (gravel to sand) the four analyzed braided rivers showed very similar spatial scaling with self-affine fractal exponents $\nu_x = 0.72$–0.77 and $\nu_y = 0.47$–0.52. This may indicate the presence of universal features in the underlying mechanisms responsible for the formation of the spatial structure of braided rivers. It is important to see whether self-affinity found in natural rivers is reproduced by a braided river model. The logarithmic correlation integral (LCI) method developed by *Sapozhnikov and Foufoula-Georgiou* [1995] enables one to test the presence of self-affinity in braided rivers and estimate the scaling exponents ν_x and ν_y. In section 4.1 a brief review of this method is presented followed by the results of self-affine analysis of natural and model-produced braided rivers. Then some additional properties of spatial patterns of braided rivers, such as island shapes, are evaluated and compared for natural and model-produced rivers.

4.1. The LCI Method for the Analysis of the Correlation Structure of Self-Affine Objects

The LCI method to test and quantitatively assess the presence of self-affinity in complex geometrical patterns, such as braided rivers, is based on the correlation integral function $M(X, Y)$, which measures the mass of an object within a rectangle (centered around a point of the object) of size $X \times Y$. For a self-affine object,
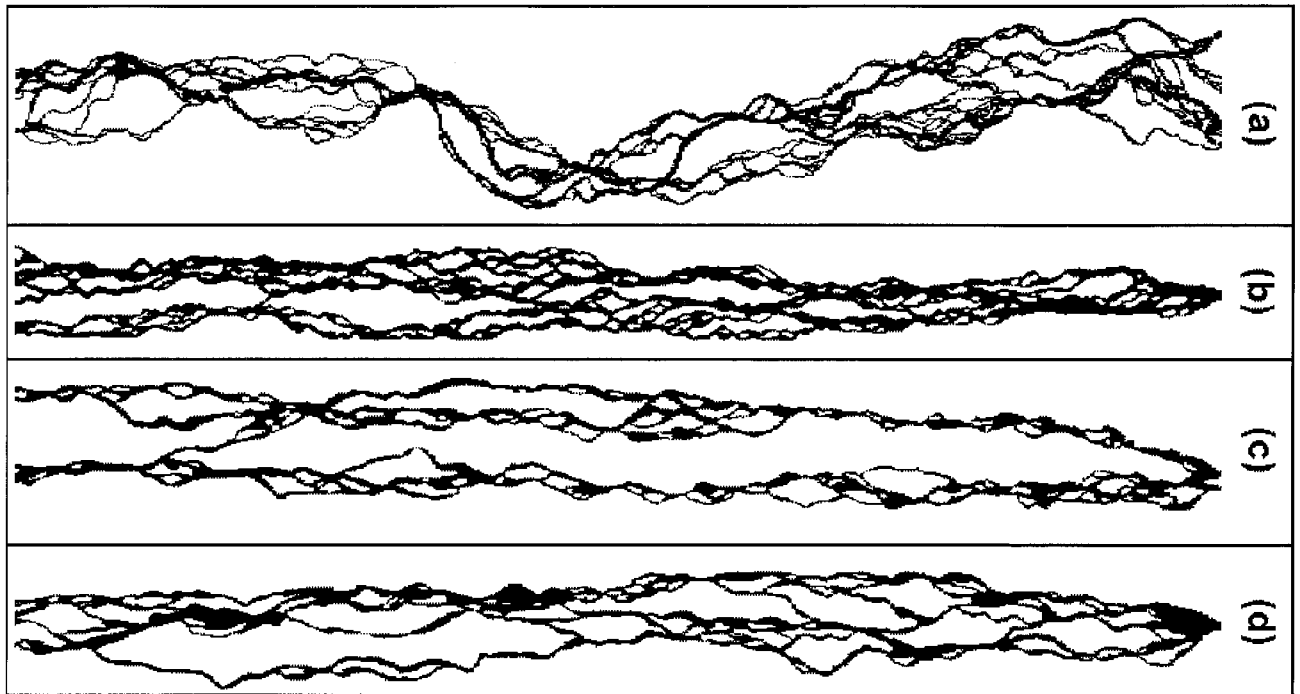
Figure 7. Digitized images of the (a) Aichilik River, (b) Q_s rule 3 model river (145,000 iterations), (c) Q_s rule 4 model river (61,000 iterations), and (d) Q_s rule 4 model river (105,000 iterations).

$$M(X, Y) \propto X^{1/\nu_x} \propto Y^{1/\nu_y} \qquad (3)$$

where ν_x and ν_y are called the fractal exponents. *Sapozhnikov and Foufoula-Georgiou* [1995] showed that the function $z(x, y) = \log (M(X, Y))$, where $x = \log (X)$ and $y = \log (Y)$, satisfies the equation

$$\nu_x \frac{\partial z}{\partial x} + \nu_y \frac{\partial z}{\partial y} = 1 \qquad (4)$$

and thus provides the means to test the presence of self-affinity in an object and estimate its fractal exponents ν_x and ν_y. Indeed, having a pattern of an object, one can estimate its logarithmic correlation integral $z(x, y)$ and use the derivatives $\partial z(x, y)/\partial x$ and $\partial z(x, y)/\partial y$ to find the values of ν_x and ν_y that satisfy (4), by a least squares method. The function $z(x, y)$ was called the logarithmic correlation integral (LCI) function, and the method was called the LCI method.

4.2. Self-Affine Scaling in Natural Braided Rivers

Application of the LCI method to the Brahmaputra, Aichilik, and Hulahula Rivers showed that (4) is satisfied for all three rivers fairly well, giving ν_x and ν_y values summarized in Table 1 together with other physical characteristics of these rivers [*Sapozhnikov and Foufoula-Georgiou*, 1996]. Interestingly, it was observed that despite the large differences in the scales of these rivers and their hydrologic properties, they all exhibited anisotropic scaling with almost the same fractal exponents ($\nu_x \simeq 0.72$ and $\nu_y \simeq 0.51$, X indicating the mainstream direction and Y the perpendicular one). This implies that if parts of a braided river are stretched by λ along the mainstream direction and by $\lambda^{\nu_y/\nu_x} \simeq \lambda^{0.7}$ along the perpendicular direction, the resulting images will look statistically similar to the each other (similarity within a braided river). At the same time, the invariance of ν_x and ν_y between braided rivers of different sizes and hydrology/sedimentology suggests

that the same anisotropic scaling as above, applied to different rivers, will result in statistically similar images, except possibly for a normalization factor to account for the different mass of each river. Such scale invariances across a range of scales, apart from being interesting in their own right, have several fundamental implications. First, they may indicate the presence of universal features in the underlying mechanisms responsible for the spatial structure of braided rivers and suggest that this structure is due to the self-organizing nature of the flow and sediment flux rather than to specific local external influences and scale. Second, knowledge of which geometric attributes are scale invariant or scale dependent is useful when applying models of braided alluvial architecture deduced from one system to another of a completely different size. Finally, since these scale invariances are properties of real braided rivers, they should also be reproduced by any model of braided river that tries to simulate realistic braided-river patterns.

4.3. Self-Affinity in the Model Braided Rivers

Braided rivers manifest salient features of their spatial structure at scales where branching comes into play, that is, scales smaller than the braid plain width. Therefore, similarly to the previous study of natural braided rivers by *Sapozhnikov and Foufoula-Georgiou* [1996], we focused on scales smaller than the braid plain width. We used the traced discharge patterns of the modeled river (and not just the patterns formed by the cells with a discharge above some threshold), similarly to the previous analysis of natural rivers and in agreement with the dynamical-systems analysis of the model performed in this work where traced images have been used.

First, a traditional fractal analysis was applied. For example, the dependence of the "mass" M (number of nonempty cells) within a square box of size R, $(M(R))$ for the river produced by the model using Q_s rule 4 (Figure 7d) is presented in Figure

8 in log-log scale. The dependence follows a straight line up to the scale of the width of the river, with a slope of 1.57. Similar analysis was applied to several runs of the model (Q_s rule 3 and Q_s rule 4). It showed that the rivers exhibit fractal behavior up to the scale of their width, with fractal dimensions $D = 1.5–1.7$ for Q_s rule 3 and $D = 1.5–1.75$ for Q_s rule 4. The values of the fractal dimensions agree with the results of *Sapozhnikov and Foufoula-Georgiou* [1996], who found fractal dimension $D = 1.5–1.6$ for three natural rivers (Aichilik, Hulahula, and Brahmaputra), *Nykanen et al.* [1998], who found $D = 1.5–1.6$ for different stages of Tanana, and *Nikora et al.* [1995], who found $D = 1.5–1.7$ for several New Zealand braided rivers.

However, this traditional fractal analysis does not show whether the object is self-similar or self-affine. Indeed, as demonstrated by *Sapozhnikov and Foufoula-Georgiou* [1995, 1996], self-affine objects (i.e., objects with scaling anisotropy) can still show linear log-log dependence $M(R)$, with slope D, which is the global fractal dimension of the self-affine object related to ν_x and ν_y as $D_G = (\nu_y - \nu_x + 1)/\nu_y$. Applying the LCI method, however, not only enabled us to study the model rivers for scaling anisotropy but also revealed other important features of the spatial structure of the rivers.

To find the fractal exponents of the model rivers, we first estimated their logarithmic correlation integrals $z(x, y)$ from the patterns of the rivers. The X axis was oriented along the slope. From the correlation integral surfaces $z(x, y)$ we calculated numerically the derivatives $\partial z(x, y)/\partial x$ and $\partial z(x, y)/\partial y$ and plotted the dependencies $\partial z(x, y)/\partial y$ versus $\partial z(x, y)/\partial x$. Figure 9 presents these dependencies for the Aichilik River [see *Sapozhnikov and Foufoula-Georgiou*, 1996], the model river using Q_s rule 4 after 61,000 iterations and the same model river after 105,000 iterations.

Let us first consider the dependence for the Aichilik River. As was shown by *Sapozhnikov and Foufoula-Georgiou* [1996],
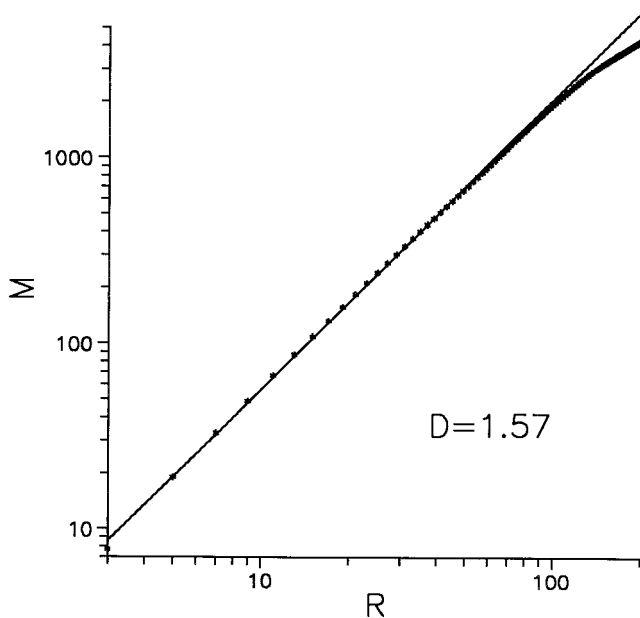
Figure 8. Spatial scaling in the Q_s rule 4, 105,000 iterations model-produced braided river indicated by the straight line log-log dependence of the "mass" M (number of nonempty cells) on the size R of the covering square box. The slope of the straight line gives the value of the fractal dimension D.
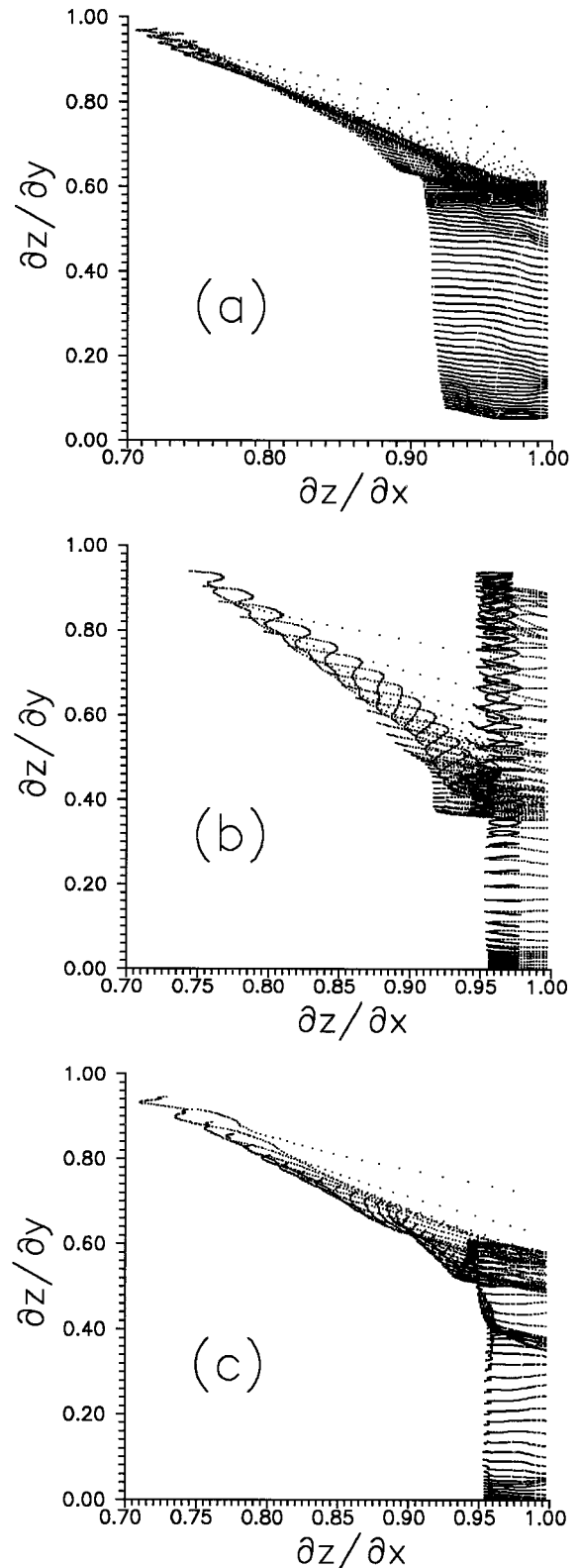
Figure 9. Dependence $\partial z(x, y)/\partial y$ versus $\partial z(x, y)/\partial x$ for (a) the Aichilik river, (b) the Q_s rule 4, 61,000 iterations model-produced river, and (c) the Q_s rule 4, 105,000 iterations model-produced river. The partial derivatives are estimated from the entire correlation integral surfaces $z(x, y)$ of the rivers.
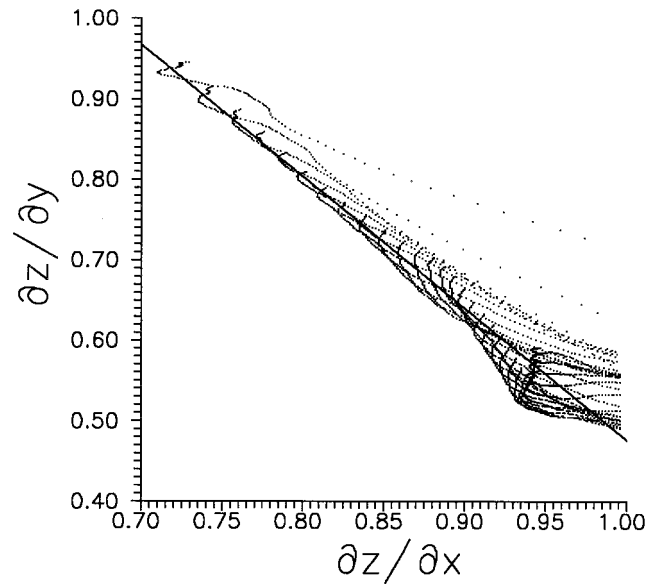
Figure 10. Estimation of the fractal exponents ν_x and ν_y for the Q_s rule 4 long run model produced river from the truncated part of the $z(x, y)$ surfaces (see text). The estimated values are $\nu_x = 0.77$ and $\nu_y = 0.47$.

the upper, linear part of the plot in Figure 9a comes from the scales up to the width of the river and indicates self-affinity in this range of scales (see equation (4)), whereas the lower part indicates a scaling break and comes from the scales exceeding the river width (similar to the scaling break in Figure 8 indicated by the deviation from the straight lines for large scales). Comparing the partial derivative plots in Figure 9, one can see that while the longer (105,000 iterations) run gives a plot quite similar to the Aichilik River (it is also similar to the plots for Brahmaputra and Hulahula shown by *Sapozhnikov and Foufoula-Georgiou* [1996]), the shorter (i.e., having undergone fewer iterations) run looks different: It has the scaling break area extending not only below but also above the log-log straight line in the plot (this feature is called here a "hat"). Similar behavior (having the "hat" appearing early in the model run and then disappearing) was observed in other model runs too. Our analysis showed that the "hat" comes from a peculiar feature of the model river at early stages: The channels tend to be parallel to each other and do not often converge. This makes the $z(x, y)$ function gain a significant magnitude at the value of y equal to the distance between the parallel channels, which leads to the high values of the partial derivatives $\partial z(x, y)/\partial y$ and forms the "hat." A close look at the pattern of the model river at the early stage (Figure 7c) confirms this conclusion. Given enough time, the model rivers evolved into a state that did not have this feature and thus became closer to natural rivers. It should be mentioned that rivers produced by Q_s rule 4 needed more time to develop the "realistic" (corresponding to natural rivers) pattern than the rivers produced by Q_s rule 3.

We then studied the linear part of the dependencies $\partial z(x, y)/\partial y$ versus $\partial z(x, y)/\partial x$ for model rivers. To check if the points in the plot where the linearity breaks come from the range of scales exceeding the river width, we cut off the part of the $z(x, y)$ surface corresponding to Y values higher than the width of the model river. Figure 10 shows the values of the

partial derivatives coming from the rest of the $z(x, y)$ function for the model river produced by Q_s rule 4 after 105,000 iterations. The points show a good linear dependence, indicating that the river exhibits spatial scaling within the scale of its width. Similar analysis was performed for other runs and for Q_s rule 3. All revealed spatial scaling up to the scales of the width of each river. Using (4), the values of the fractal exponents were found to be $\nu_x = 0.72$–0.78 and $\nu_y = 0.40$–0.54 for Q_s rule 3 and $\nu_x = 0.75$–0.97 and $\nu_y = 0.47$–0.52 for Q_s rule 4. The scaling anisotropy was $\nu_x/\nu_y = 1.46$–1.95 for Q_s rule 3 and $\nu_x/\nu_y = 1.44$–1.88 for Q_s rule 4. These results imply that the model rivers are self-affine objects showing a high degree of anisotropy.

One can see that while the fractal dimension of the model rivers is close to that of the studied natural rivers, the anisotropy parameter ν_x/ν_y is on the average higher for the modeled rivers (1.44–1.95 versus 1.41–1.60 for the four studied natural rivers). It should be noted that the spread of the scaling parameters is higher in modeled rivers (especially for Q_s rule 4) than for natural rivers.

4.4. Island Shape Comparison

The LCI method reveals the scaling anisotropy of an object as a whole. Here we also studied the sizes of islands in the modeled rivers for scaling anisotropy. The size of each island in the direction of the slope, l_x, and in the perpendicular direction, l_y, was estimated as the root-mean-square of the deviation (in the corresponding direction) of pixels constituting the island from the center of mass of the island: $l_x = [(1/n)\sum_{i=1}^{n}(\bar{X} - X_i)^2]^{1/2}$ and $l_y = [(1/n)\sum_{i=1}^{n}(\bar{Y} - Y_i)^2]^{1/2}$, where n is the number of pixels in the island. Figure 11 shows the log-log plot of the sizes of the islands l_x and l_y in the X and Y directions, respectively, for the model river produced using Q_s rule 4 and after 105,000 iterations. The log-log linearity of the l_y versus l_x dependence indicates scaling. The slope of the log-log linear dependence is equal to 1.35. The fact that the slope is different from 1 indicates anisotropy in scaling of the islands in X and Y directions. The analysis of islands for scaling was performed for other runs of the model (both Q_s-rule 3 and
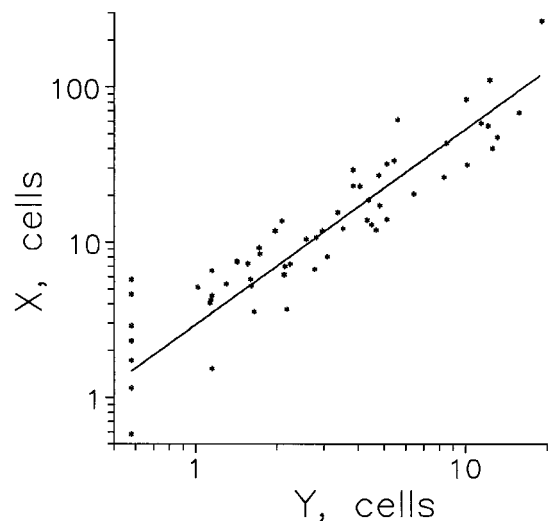

Figure 11. Scaling in the projections of the islands on the X and Y axes in the Q_s-rule 4, 105,000 iterations model produced river. The estimated value of the slope is 1.35, which is different from 1 indicating scaling anisotropy.

Q_s-rule 4). In all cases, anisotropic scaling of islands was found.

It should be noted that the scaling anisotropy of the islands was 10–20% lower than the scaling anisotropy of the modeled rivers as a whole obtained by the LCI method. This is in agreement with the results obtained previously by *Sapozhnikov and Foufoula-Georgiou* [1996] for natural rivers, where the scaling anisotropy of the sizes of islands in a river was also found to be 10–20% lower than the anisotropy of the river as a whole. In our opinion this difference implies that the scaling anisotropy of a braided river is only partially reflected by the anisotropy of islands. Part of the anisotropy in a braided river stems from the anisotropy in tortuosity of the river (same as anisotropy in tortuosity of single-channel rivers causing their scaling anisotropy). These two factors exist on scales that overlap and therefore cannot be separated.

5. Discussion and Conclusions

The state-space and the scaling analyses proposed here for braided river model validation complement each other. Indeed, the state-space analysis characterizes the river pattern in the dynamical-system theory framework, enabling one to follow how the total width of the river changes downstream. For example, the state-space analysis easily distinguishes sudden changes in the river width from gradual ones. Moreover, it shows whether abrupt or gradual changes occur more frequently in narrow or in wide sections: For example, compare the state-space plot of the Hulahula River (Figure 3a), showing abrupt changes (big loops) only in wide sections of the river, with the state-space plot of a run of the model river (Figure 3d), showing abrupt changes in both narrow and wide sections. The scaling analysis via the logarithmic correlation integral (LCI) method, on the other hand, characterizes correlation properties of the multiscale spatial structure of a braided river in different directions and reveals anisotropic scaling (self-affinity) in the river, something which the state-space analysis was not designed for. Besides, the state-space-plot method uses the total width at each cross section of the river. Therefore it does not include information of the width, shape, and relative position of the individual channels. These important characteristics of a braided river are reflected in the correlation structure of the river and captured by the LCI analysis. In fact, as we demonstrated in this article, the analysis of the correlation structure of braided rivers by the LCI method discloses subtle differences between the structure of the simulated and natural river patterns (such as, for example, the fact that channels of the modeled rivers tend to be more parallel at early stages of the model runs than at later stages and in natural rivers (see Figure 9)). Together the two methods provide a fairly comprehensive approach to testing how realistic a model-produced river pattern is. They reveal and quantify subtle characteristics of the river pattern, and thus they permit testing a model and determining the most realistic rules and parameters of that model.

The analysis of the modeled rivers using the cellular model of *Murray and Paola* [1994] showed that they eventually develop into a state exhibiting anisotropic spatial scaling (self-affinity). This is in agreement with the results of the analysis of natural braided rivers presented by *Sapozhnikov and Foufoula-Georgiou* [1996]. The presence of spatial scaling in natural braided rivers (which implies absence of a preferred scale) was interpreted by *Sapozhnikov and Foufoula-Georgiou* [1996] as a

strong indication that the same physical mechanisms are responsible for the formation of braided pattern at different spatial scales, from the scale of the smallest channel to the scale of the braid plain width. The fact that model rivers, after they are left to evolve long enough, also exhibit spatial scaling definitely supports the validity of the model. Moreover, scaling anisotropy of natural braided rivers due to gravity is also present in model rivers, which also speaks in favor of the model. It should be mentioned that although the scaling anisotropy of modeled rivers is not very far from that of natural rivers, it is somewhat higher. We believe that the higher value of the scaling anisotropy parameter ν_x/ν_y in the modeled rivers is (at least partially) due to the fact that because of the restrictions of the simulated basin width they were forced to be rectilinear as a whole. The presence of the long-scale sinuosity in natural braided rivers (unless they are restricted by natural constraints) is an important component of their geometry which obviously produces a lower scaling anisotropy compared to the situation when the whole structure is strictly oriented in one direction. It remains to be determined whether the higher anisotropy of the modeled rivers is caused only by different external conditions (the imposed rectilinear shape of the basin) or is also due to the imperfection of the rules of the model. Also, the scaling anisotropy parameter shows higher variance for modeled rivers (1.44–1.95) than for the studied natural rivers (1.41–1.60). We believe this is due to the restricted size of the grid-modeled rivers, which lead to modeled rivers with fewer channels than the natural rivers and, correspondingly, more statistical noise.

In braided rivers, deep narrow sections of the river, which can carry more sediment and therefore cause erosion, are followed by wider and shallower sections where deposition occurs. The current loses much of its sediment in such divergent shallow sections and thus is capable of eroding the bed downstream, producing again a deep and narrow section. State-space analysis shows how such wide shallow and deep narrow sections of a river follow each other. Since these sequences are governed by the processes controlling deposition and erosion of the river, comparison of state-phase plots of modeled rivers with natural ones can tell us if the important features of the physical mechanisms in braided rivers are captured by the model. Our state-space analysis shows that for both Q_s rules 3 and 4, model realism depends on the parameters of the model (e.g., compare Figures 3d and 3e, or see Figure 5). For the best values of parameters the normalized distance between modeled rivers and natural rivers is not very much higher than the distance between the natural rivers themselves. This indicates that the physical mechanisms responsible for the geometry of braided rivers are mainly represented in the model (although some difference between modeled and natural rivers still remains). Our results suggest that model behavior is not sensitive to the difference between Q_s rules 3 and 4. In our opinion, this indicates that once physical mechanisms allow sediment to be transported over flat slopes (which is important), the details of how it happens are not critical. It should be noted, however, that some differences may still exist. Thus our fractal analysis of the spatial structure of the model rivers at different moments in time reveals that rivers produced by Q_s rule 4 needed more time to develop the "realistic" pattern (i.e., the pattern showing spatial scaling as natural rivers do) than the rivers produced by Q_s rule 3.

Although we believe that the state-space analysis and the self-affine fractal analysis presented in this paper together

make up a fairly comprehensive test for validating braided rivers models, there are other important issues not reflected in this analysis. We think that at least three other features of modeled braided rivers should be compared to natural ones: (1) the terrain produced by the river, (2) the hydrology of the river (e.g., distribution of the discharge between the channels), and (3) the evolution of the river (e.g., it was shown by *Sapozhnikov and Foufoula-Georgiou* [1997] that braided rivers exhibit dynamic scaling, an indicator of self-organized criticality). This work is currently under development.

References

Ashmore, P., Process and form in gravel braided streams: Laboratory modelling and field observations, Ph.D. thesis, Univ. of Alberta, Edmonton, 1985.

Blondeaux, P., and G. Seminara, A unified bar-bend theory of river meanders, *J. Fluid Mech.*, *157*, 449–470, 1985.

Dudley, R. M., Probabilities and metrics, *Lecture Note Ser. 45*, Mat. Insti. Arhus Univ., Arhus, Denmark, 1976.

Dudley, R. M., *Real Analysis and Probability*, Wadsworth, Belmont, Calif., 436 pp., 1989.

Fredsoe, J., Meandering and braiding of rivers, *J. Fluid Mech.*, *84*, 609–624, 1978.

Frish, U., B. Hasslacher, and Y. Pomeau, Lattice-gas automata for Navier-Stokes equation, *Phys. Rev. Lett.*, *56*, 1505–1508, 1986.

Hutchinson, J. E., Fractals and self-similarity, *Indiana Univ. Math. J.*, *30*, 713–747, 1981.

Kaneko, K., *Theory and Applications of Coupled Map Lattices*, 189 pp., John Wiley, New York, 1993.

Miller, R. G., Jr., *Beyond Anova: Basics of Applied Statistics*, 317 pp., John Wiley, New York, 1986.

Moeckel, R., and A. B. Murray, Measuring the distance between time series, *Physica D*, *102*, 187–194, 1997.

Murray, A. B., and C. Paola, A cellular automata model of braided rivers, *Nature*, *371*, 54–57, 1994.

Murray, A. B., and C. Paola, A new quantitative test of geomorphic models applied to a model of braided streams, *Water Resour. Res.*, *32*(8), 2579–2587, 1996.

Murray, A. B., and C. Paola, Properties of a cellular braided stream model, *Earth Surf. Processes Landforms*, *22*, 1001–1025, 1997.

Nikora, V. I., D. M. Hicks, G. M. Smart, and D. A. Noever, Some fractal properties of braided rivers, paper presented at 2nd International Symposium on Fractals and Dynamic Systems in Geoscience, Univ. of Frankfurt, Frankfurt/Main, Germany, April 4–7, 1995.

Nykanen, D. K., E. Foufoula-Georgiou, and V. B. Sapozhnikov, Study of spatial scaling in braided river patterns using synthetic aperture radar imagery, *Water Resour. Res.*, *34*(7), 1795–1807, 1998.

Parker, G., On the cause and characteristic scales of meandering and braiding in rivers, *J. Fluid Mech.*, *76*, 457–480, 1976.

Parker, G., Self formed rivers with equilibrium banks and mobile bed, 2, The Gravel River, *J. Fluid Mech.*, *89*, 127–146, 1978.

Parker, G., Lateral bed load transport on side slopes, *J. Hydrol. Eng.*, *110*, 197–199, 1984.

Salem, J., and S. Wolfram, Thermodynamics and hydrodynamics of cellular automata, in *Theory and Applications of Cellular Automata*, edited by S. Wolfram, pp. 326–366, World Sci., River Edge, N. J., 1986.

Sapozhnikov, V. B., and E. Foufoula-Georgiou, Study of self-similar and self-affine objects using logarithmic correlation integral, *J. Phys. A Math. Gen.*, *28*, 559–571, 1995.

Sapozhnikov, V. B., and E. Foufoula-Georgiou, Self-affinity in braided rivers, *Water Resour. Res.*, *32*, 1429–1439, 1996.

Sapozhnikov, V. B., and E. Foufoula-Georgiou, Experimental evidence of dynamic scaling and indications of self-organized criticality in braided rivers, *Water Resour. Res.*, *33*, 1983–1991, 1997.

Sauer, T. J., J. A. York, and M. Casdagli, Embedology, *J. Stat. Phys.*, *65*, 579–616, 1991.

Sugihara, G., Nonlinear forecasting for the classification of natural time series, *Philos. Trans. R. Soc. London*, *Ser. A*, *348*, 477–495, 1994.

Takens, F., Detecting strange attractors in turbulence, in *Dynamical Systems and Turbulence*, edited by D. A. Rand and L. S. Young, pp. 366–381, Springer-Verlag, New York, 1981.

Tennekes, H., and J. L. Lumley, *A First Course in Turbulence*, 300 pp., MIT Press, Cambridge, Mass., 1990.

Toffoli, T., Cellular automata model as an alternative to (rather than approximation of) differential equations in modeling physics, *Physica D*, *10*, 117–127, 1984.

Vichniac, G., Simulating physics with cellular automata, *Physica D*, *10*, 96–115, 1984.

Weigend, A. S., and N. A. Gershenfeld (Eds.), *Time Series Prediction: Forecasting the Future and Understanding the Past*, SFI Stud. Sci. Complexity, 630 pp., Addison-Wesley, Reading, Mass., 1994.

Wolman, M. G., A method of sampling coarse riverbed material, *Eos Trans. AGU*, *35*, 951–956, 1954.

E. Foufoula-Georgiou and V. B. Sapozhnikov, Department of Civil Engineering, St. Falls Laboratory, University of Minnesota, Mississippi River at Third Avenue, SE, Minneapolis, MN 55414-2196. (e-mail: efi@mykonos.safhl.umn.edu; victor@mykonos.safhl.umn.edu)

A. B. Murray and C. Paola, Department of Geology and Geophysics, University of Minnesota, Minneapolis, MN 55455. (e-mail: brad@beaches.ucsd.edu; cpaola@maroon.tc.umn.edu)